Journal of Alloys and Compounds 1004 (2024) 175832

Contents lists available at ScienceDirect

Journal of Alloys and Compounds

journal homepage: www.elsevier.com/locate/jalcom

Effects of hydrazine compounds as additives on the characteristics of organic-inorganic hybrid lead-tin perovskite photovoltaic device

Kai-Leng Huang [a], Chia-Feng Li [a], Yu-Chi Chen [a], Sheng-Wen Huang [b], Yu-Ching Huang [b], Wei-Fang Su [b], Feng-Yu Tsai [a,*]

[a] Department of Materials Science and Engineering, National Taiwan University, Taipei 10617, Taiwan, ROC
[b] Department of Materials Engineering, Ming Chi University of Technology, Taipei 24301, Taiwan, ROC

ARTICLE INFO

Keywords:
Organic-inorganic hybrid lead-tin perovskite solar cells
Low bandgap perovskite solar cells
Additive engineering
Stability
Semiconductor devices

ABSTRACT

Lead-tin perovskite solar cells (Pb-Sn PSCs) are a more environmentally friendly alternative to the mainstream lead-based PSCs, but their development has been hampered by their instability due to the strong tendency of the Sn^{2+} constituent to oxidize. This study examines the effects of three types of hydrazine compound—phenylhydrazine hydrochloride (PH•HCl), 4-fluorophenylhydrazine hydrochloride (FPH•HCl), and 1-[2,5-bis(trifluoromethyl)phenyl]hydrazine hydrochloride (BTFMPH•HCl)—as additives to Pb-Sn perovskite precursor solutions on the stability and performance of Pb-Sn PSC devices, taking advantages of the hydrazine functional group's ability to suppress oxidation of Sn^{2+}, and of the hydrophobicity provided by the phenyl structure and/or fluorine (F) contents of the selected compounds. All of the three additives significantly improved the stability of the resultant Pb-Sn PSC devices, with the additives containing more F contents (BTFMPH•HCl > FPH•HCl > PH•HCl) showing slightly greater improvements. The PH•HCl additive markedly enhanced the power conversion efficiency (PCE) while reducing the hysteresis ratio of the PSC devices thanks to its multifaceted effects including improving morphology, reducing non-radiative losses, alleviating recombination defects, and enhancing charge-carrier mobility of the Pb-Sn perovskite layer, as elucidated by a series of photo-luminescence and electrical characterizations. Both the BTFMPH•HCl and FPH•HCl additives slightly degraded the device PCE due to their poorer resultant perovskite morphology, which was attributed to their lower affinity with the perovskite as a result of their F contents. Our results provide useful insights in selecting and designing hydrazine-based additives for PSC.

1. Introduction

Organic-inorganic hybrid perovskite solar cells (PSCs) are a promising type of photovoltaic devices thanks to their advantages including high power conversion efficiency (PCE), low-cost ingredients, and ease for scaled-up production [1,2]. One major area of development for PSCs technologies is to decrease or eliminate the Pb content of the mainstream Pb-based perovskite photo-absorber materials of PSCs, so as to minimize the potential environmental impacts of the Pb content. Among the approaches for Pb reduction of PSCs, partially replacing the Pb content with Sn—forming so-called Pb-Sn PSCs—has been particularly attractive, as it is capable of preserving the high PCE of Pb-based PSCs, which has proven to be a difficult task for other Pb-reduction approaches [3–5]. Despite the high PCE achievable with Pb-Sn PSCs, however, the practical viability of Pb-Sn PSCs, and by extension Sn-based PSCs, is still severely limited by the strong susceptibility of the Sn content to oxidize from the desired Sn^{2+} form to the detrimental Sn^{4+} form [6]. Prior efforts have identified two main methods for alleviating this issue: (1) adding reducing or oxidation-suppressing agents into perovskite precursor solutions—such as Sn powders, SnF_2, hypophosphorous acid, and hydrazine halides [6–11]—to suppress Sn^{2+} oxidation; (2) introducing additives that provide bulky cations, preferably ones with hydrophobic substituents, to passivate the crystal grain boundaries in perovskite films and block moisture incursion. Hydrazine compounds have been shown to be a particularly advantageous type of additives because they are capable of providing both of the above-mentioned functions by serving simultaneously as reducing agents and bulky cations, allowing for remarkable enhancements in performance of Pb-Sn and Sn-based PSCs [12–16]. Although impressive PCE and stability have been demonstrated for hydrazines-modified Pb-Sn and Sn-based PSCs, the variety of

* Corresponding author.
E-mail address: ftsai@ntu.edu.tw (F.-Y. Tsai).

https://doi.org/10.1016/j.jallcom.2024.175832
Received 14 December 2023; Received in revised form 18 July 2024; Accepted 2 August 2024
Available online 3 August 2024

hydrazine compounds that has been studied is still quite limited, and therefore the effects of varying the chemical structures of hydrazine compounds on the performances of hydrazines-modified PSCs have not been elucidated.

This study examined three hydrazine compounds with related structures as additives for Pb-Sn PSCs, which included phenylhydrazine hydrochloride (PH•HCl), 4-fluorophenylhydrazine hydrochloride (FPH•HCl), and 1-[2,5-bis(trifluoromethyl)phenyl]hydrazine hydrochloride (BTFMPH•HCl). The selected hydrazine compounds are derivatives of phenylhydrazine (PH) with various numbers of fluorine substituents including zero (PH•HCl), one (FPH•HCl), and six (BTFMPH•HCl), whose chemical structures are shown in Fig. 1. (a-c) along with a schematic drawing of the Pb-Sn PSC device architecture used herein. Of the three selected compounds, PH•HCl has been reported to significantly improve the stability and PCE of Sn-based PSCs, thanks to its phenyl moiety's hydrophobicity and bulkiness in addition to the reducing ability of the hydrazine functional group [13]. Building upon this concept, this study explored the effects of PH•HCl additive on the device characteristics of Pb-Sn PSCs as well as the effects of having different numbers of fluorine substituents on the PH•HCl base structure, where the fluorine substituents were expected to contribute additional hydrophobicity for potential further enhancement of device stability against environment-induced degradations. The additive concentration of each of the hydrazine compounds was optimized in terms of Pb-Sn PSC device metrics, which were then compared to examine the differences in additive performance among the three tested compounds. The morphologies, surface properties, and charge-carrier generation and transport characteristics of the hydrazine-modified Pb-Sn PSCs were analysed to determine the mechanisms through which the hydrazine additives imparted their effects.

2. Experimental section

2.1. Materials

Fluorine-doped tin oxide (FTO, 5–7Ω, SKU: RL39) was purchased from Rui Long Optoelectronics Inc. Formamidinium iodide (FAI, 99.99 % purity, SKU: MS150000) was purchased from Greatcell Solar Materials Inc. Poly(3,4-ethylenedioxythiophene) polystyrene sulfonate (PEDOT:PSS) aqueous solution (Clevious PVP AI 4083) was purchased from Heraeus Inc. and filtered through a 0.45 μm PTFE hydrophilic filter (Dinhaw Enterprise Inc., SKU: SLCR033) before use. Cesium iodide (CsI, 99.999 % purity, SKU: 429384), tin (II) iodide (SnI_2, 99.99 % purity, SKU: 409308), tin fluoride (SnF_2, 99 % purity, SKU: 334626), dimethyl sulfoxide (DMSO, ≧99.9 % purity, SKU: 276855), N,N-dimethylformamide (DMF, 99.8 % purity, SKU: 227056), chlorobenzene (CB, 99.8 % purity, SKU: 284513), phenylhydrazine hydrochloride (PH•HCl, ≧99 % purity, SKU: 114715), 4-fluorophenylhydrazine hydrochloride (FPH•HCl, 97 % purity, SKU: F14203) and 1-[2,5-bis(trifluoromethyl)phenyl]hydrazine hydrochloride (BTFMPH•HCl, SKU: PH018984) were purchased from Sigma-Aldrich Inc. Lead iodide (PbI_2, 99.99 % purity, SKU: L0279) was purchased from Tokyo Chemical Industry Inc. Fullerene (C_{60}, >99.9 % purity, SKU: LT-S903), 2,9-dimethyl-4,7-diphenyl-1,10-phenanthroline (BCP, >99.5 % purity, SKU: LT-E304H) and [6,6]-Phenyl C_{61} butyric acid methyl ester ($PC_{61}BM$, >99 % purity, SKU: LT-S905) were purchased from Luminescence Technology Inc.

2.2. Preparations of perovskite precursor solutions

The perovskite precursor solutions were prepared in a nitrogen-filled glovebox (< 0.5 ppm O_2 and < 0.5 ppm H_2O). The precursor solutions contained 1.6 M of $Cs_{0.25}FA_{0.75}Pb_{0.5}Sn_{0.5}I_3$, which was made up of a stoichiometric ratio of 103.9 mg CsI, 206.4 mg FAI, 369.6 mg PbI_2, 298 mg SnI_2 in a 1 ml solvent mixture consisting of DMF and DMSO in a 3:1 vol ratio (DMF: DMSO=3:1 v/v), with added SnF_2 (10 mol% relative to SnI_2). The solution was stirred at room temperature for 1 h and then filtered through a 0.45 μm PTFE filter before use. To prepare additive-added perovskite samples, a given amount of each of the three additives, PH•HCl, FPH•HCl, and BTFMPH•HCl, was added to the 1.6 M $Cs_{0.25}FA_{0.75}Pb_{0.5}Sn_{0.5}I_3$ precursor solution to reach the desired additive concentration, which was in percentage molar ratio against the $Cs_{0.25}FA_{0.75}Pb_{0.5}Sn_{0.5}I_3$ host. For example, to prepare a 2 mol% additive-added perovskite sample with one of the hydrazine additives, 4.6 mg of PH•HCl, 5.0 mg of FPH•HCl, or 9.0 mg of BTFMPH•HCl was added to 1 ml of the 1.6 M $Cs_{0.25}FA_{0.75}Pb_{0.5}Sn_{0.5}I_3$ precursor solution.

2.3. Device fabrication

The device fabrication steps used in this work were as follows: (1) ultrasonically cleaning a FTO glass substrate for 10 min in turn in a soap/water solution, acetone, methanol, and isopropanol, followed by blow-drying with N_2 and a 10 min UV-ozone pre-treatment; (2) spin-coating a PEDOT:PSS hole-transporting layer (HTL) from 140 μL of the

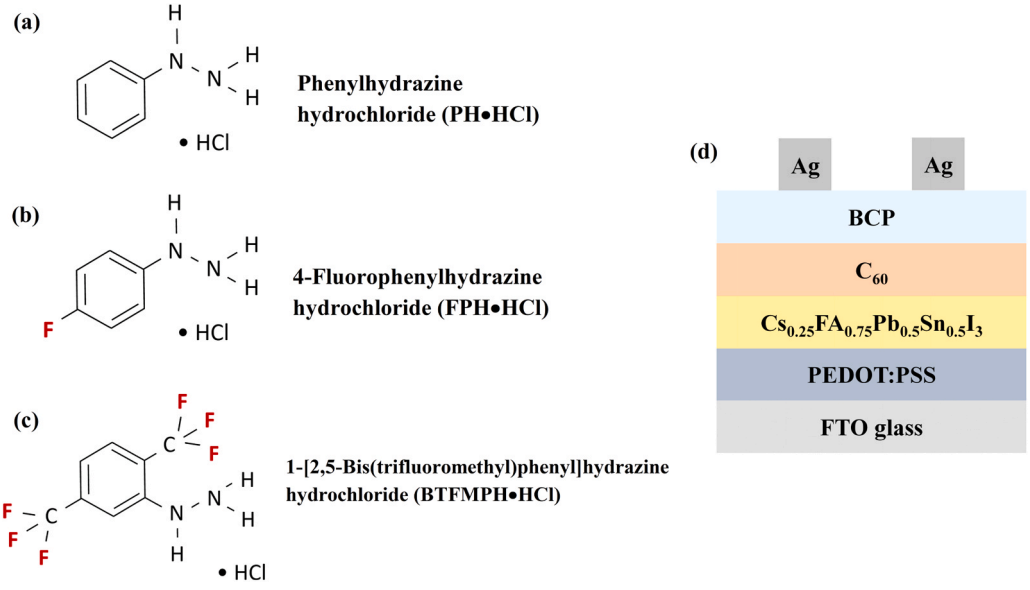

Fig. 1. (a-c) Chemical structures of the selected hydrazine compounds; (d) illustration of the architecture of the Pb-Sn PSC devices used herein.

PEDOT:PSS solution at 4000 r.p.m. for 30 s followed by baking first at 150 °C for 10 min in ambient air and then at 150 °C for 5 min in a nitrogen-filled glovebox; (3) with the sample remaining in the glovebox, spin-coating a perovskite layer from 140 μL of one of the perovskite solutions at 1000 r.p.m. for 10 s and then 4000 r.p.m. for 40 s, during the latter of which 500 μL of chlorobenzene was dripped onto the spinning substrate starting at the 21st second and continuing through the end of the spin-coating step, followed by baking on a hotplate at 100 °C for 10 min; (4) thermally evaporating in turn a 30 nm-thick C_{60}, a 7 nm-thick BCP, and a 100 nm-thick Ag layer through a shadow mask in a thermal evaporator housed in the glovebox. The device architecture is illustrated in Fig. 1(d).

2.4. Materials and device characterizations

Photovoltaic characteristics of the PSC devices were measured with a Keithley 2410 voltage source meter and a Yamashita Denso YSS-50A-400A solar simulator providing an illumination of AM 1.5 G solar spectrum at a light intensity of 100 mW/cm^2. Instruments used for various materials characterization are listed as follows: contact angle measurements: Sindatek Model 100SB; scanning electron microscopy (SEM): Hitachi S4800; atomic force microscopy (AFM): Bruker OMV-NTSC; UV/visible spectroscopy: JASCO V-770; external quantum efficiency (EQE): PV Measurements QEX10; X-ray diffraction (XRD): Bruker D2 PHASER XE-T with Cu-Kα radiation of =1.54 Å; photoluminescence (PL) and time-resolved PL (TRPL): Edinburgh Instruments FLS1000; electrochemical impedance spectroscopy (EIS): FLUXiM Paios; film-thickness measurements: KLA D-300. Space charge limited current (SCLC) measurements were performed on hole- and electron-only devices using a Keysight Agilent B1500A measurement system, where the hole- and electron-only devices had the following structures, respectively: FTO/PEDOT:PSS/PVKs/Ag and FTO/PC_{61}BM/PVKs/C_{60}/BCP/Ag.

3. Results and discussions

3.1. Reducing strength and hydrophobicity of the hydrazine additives

The ability of the three types of hydrazine additives to reduce oxidized Sn^{4+} in Pb-Sn perovskite precursor solutions was evaluated by observing the change in color of the precursor solutions exposed to the ambient air, following the methodology reported in previous works [6,7,17]; and the results are shown in Fig. 2(a-c). The pristine Pb-Sn perovskite precursor solutions exhibited the characteristic yellow color, which darkened into a reddish color upon exposure to the ambient air due to oxidation of the Sn^{2+} in the solutions to Sn^{4+}. Upon addition of each of the three hydrazine additives, the solutions immediately recovered their original yellow color, which indicated that all of the three hydrazine compounds readily reduced the air-exposure-generated Sn^{4+}back to Sn^{2+}. The reaction scheme of the reduction reaction has been shown to be as follows [12]:

$$R\text{-}NHNH_2 + 2Sn^{4+} \rightarrow R\text{-}N{\equiv}N^{+} + 2Sn^{2+} + 3\,H^{+} \quad (1.1)$$

During the subsequent continuous air-exposure for up to 1 week, however, the rate at which the solutions' color darkened again—as a result of re-oxidation of Sn^{2+} to Sn^{4+}— was different with the three hydrazine compounds. All of the three hydrazine-added solutions exhibited a much slower darkening than did the pristine solution, which again evidenced the reducing effects of the three hydrazine additives. Among the three hydrazine-added solutions, the solutions with the F-containing hydrazines, namely FPH•HCl and BTFMPH•HCl, showed faster darkening (i.e. more rapid re-oxidation) than did the solution with the F-free PH•HCl. The faster re-oxidation of the FPH•HCl- and BTFMPH•HCl-added solutions was attributed to the strong electron-withdrawing tendency of the F substituents of the two hydrazines, which lowered the reducing strength of their neighboring hydrazine functional group. The reducing ability of the hydrazine additives was verified with XPS analysis on perovskite films with or without the addition of the additives, as shown in Fig. S1, where the hydrazine-added perovskite films showed significantly lower Sn^{4+} content than the pristine film.

Fig. 2(d-g) present the water contact angles of Pb-Sn perovskite films before and after the addition of either one of the three hydrazines. All of the three hydrazine additives noticeably increased the water contact angle, with the effect more pronounced for the hydrazines with higher amounts of F, i.e. BTFMPH•HCl > FPH•HCl > PH•HCl. The increases in water contact angle reflected the hydrophobicity of the phenyl structure and the F substituents of the hydrazines, while the trend in the water contact angles indicated the effects of the number of F substituents, i.e. the more the F substituents, the higher the water contact angles of the Pb-Sn perovskite films.

3.2. Effects of the hydrazine additives on Pb-Sn PSC devices characteristics

The optimal concentration for each of the three hydrazine additives in the perovskite precursor solutions was determined in terms of PCE of the Pb-Sn PSC devices, as shown in Fig. 3. The optimal concentration was found to be 2, 2, and 0.25 mol% for PH•HCl, FPH•HCl, and BTFMPH•HCl, respectively. The lower optimal concentration of BTFMPH•HCl was attributed to BTFMPH•HCl's high F content and large molecular size, which would lower its solubility and compatibility in perovskites.

The Pb-Sn PSC device characteristics resulting from each of the three hydrazine additives at their respective optimal concentration are compared in Fig. 4(a-e) and Table 1. The J_{SC} values measured with the

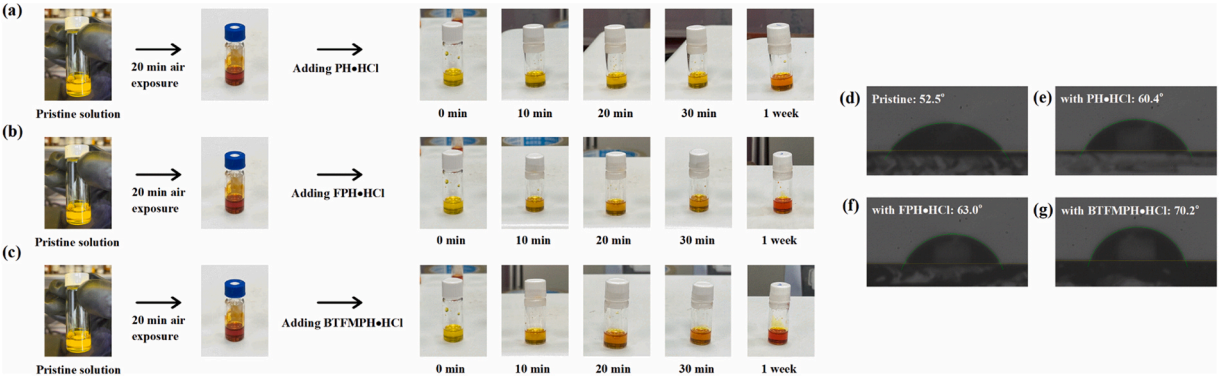

Fig. 2. (a-c) Photographs of $Cs_{0.25}FA_{0.75}Pb_{0.5}Sn_{0.5}I_3$ precursor solutions during exposure to ambient air before and after the addition of the hydrazine additives; (d-g) photo-images of water contact angle measurements on Pb-Sn perovskite films with and without the addition of hydrazine additives.

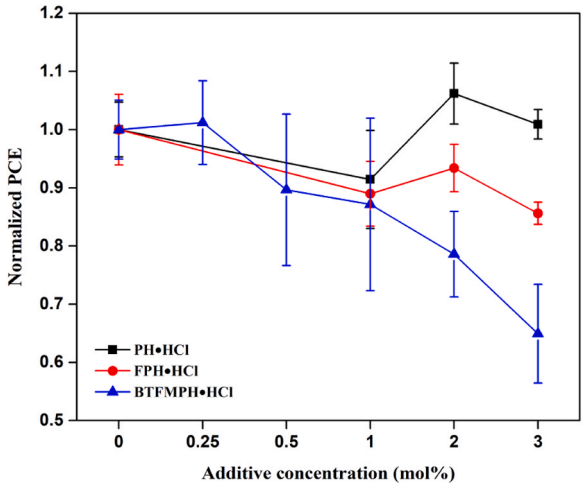

Fig. 3. Normalized Pb-Sn PSC device PCE resulting from different added concentrations of PH•HCl, FPH•HCl, or BTFMPH•HCl; normalization was against the PCE of the control devices, which were free of the hydrazine additives.

solar simulator were verified with EQE measurements, as shown in Fig. 4 (f). It can be seen from the presented results that of the three hydrazine additives, only PH•HCl noticeably improved the PSC device characteristics, with the other two additives either slightly degraded or maintained similar device characteristics. The hysteresis behaviors of the PSC devices were quantified in terms of the hysteresis ratio, which was the difference between a device's reverse-scanning and forward-scanning PCE's as a fraction of the reverse-scanning PCE, and the calculated hysteresis ratios are included in Table 1. Of the three hydrazine additives, both PH•HCl and FPH•HCl significantly lowered the hysteresis ratio, while BTFMPH•HCl sizably raised the hysteresis ratio.

The effects of each of the hydrazine additives on the stability of Pb-Sn PSC devices were examined by measuring the device PCE as a function of storage time in humid air (~25 °C and ~70 % RH), and the results are presented in Fig. 5. Owing to the Pb-Sn PSC's inherent susceptibility to moisture and oxygen, the PSC devices degraded rapidly in the humid-air testing condition; however, all of the three hydrazine additives effectively slowed the rate of the air-induced degradation, with the effects slightly stronger for the additives with higher F content, i.e. BTFMPH•HCl > FPH•HCl > PH•HCl. This trend indicated that between the opposing effects of F content, i.e. lowering the reducing strength but increasing the hydrophobicity of a hydrazine, the latter was more dominant in determining the stability of a hydrazine-added device. The long-term storage stability of the devices was also tested in a N_2-filled glove box, as shown in Fig. S2. The control device (without additive) showed a similar degradation profile to those reported previously for Pb-Sn PSCs [18], while the additive-containing devices exhibited much slower decay after 4 months of storage.

3.3. Mechanisms of the effects of the hydrazine additives

The results presented above confirmed that the three hydrazine additives served their expected function of improving device stability, through acting both as reducing agents against environment-induced oxidation and as hydrophobic components against moisture-induced degradations. The F-content had opposing effects on the reducing strength and hydrophobicity, i.e. diminishing reducing strength while enhancing hydrophobicity, and as a result the three additives showed only slight differences in their resultant device stability.

XRD analysis results provided in Fig. S3 showed that the diffraction patterns of the Pb-Sn perovskite layers did not noticeably change with the addition of either of the three additives, indicating that the additives were not incorporated into the perovskite crystals but instead were located at the grain boundaries, consistent with previously reported observations on additives-modified perovskites [19]. XPS analysis (Fig. S1) indicated that the additives likely formed complexes with Sn^{2+} in the grain boundaries, as the addition of the additives caused the Sn^{2+} peaks in XPS to blue-shift slightly [18]. Similarly, addition of the three additives did not noticeably alter the UV–vis absorption spectra (Fig. S4) of the perovskite films, resulting in similar optical band gaps and absorbance. FTIR analysis (Fig. S5) also present consistent findings, where the additives did not cause detectable change in FTIR spectrum. SEM analysis results presented in Fig. 6(a-l) (cross-sectional SEM images are presented in Fig. S6), on the other hand, revealed that the additives changed the average grain size on the surface of the Pb-Sn perovskite films. Specifically, addition of PH•HCl increased the average grain size, while addition of either FPH•HCl or BTFMPH•HCl reduced it, with the former only slightly and the latter more significantly. The grain-size-reducing effects of FPH•HCl and BTFMPH•HCl were attributed to their lower solubility in the Pb-Sn perovskite stemming from their F substituents, which would increase the rate of nucleation during the film-forming process; the effects were more pronounced for BTFMPH•HCl as a result of its greater F content. It should be noted that the grain sizes in these additive-modified perovskite films were also determined with XRD (Fig. S3), which, however, showed that grain sizes were similar among the without-additive and with-additive perovskite films. The apparent contradiction between the XRD and SEM results indicated that the grain-size difference was likely confined to the surface layer of the PVSK films, which was also suggested by the SEM cross-sectional images presented in Fig. S6.

In light of these observed morphological differences, it may be inferred that the enhanced PCE of the PH•HCl-added devices were owing to the increased average grain size and reduced grain boundaries at the top surface of the perovskite layer, where the additive would serve to passivate charge-recombination defects (to be verified in further analysis discussed below) [20–22]. Likewise, the negative effects of FPH•HCl and BTFMPH•HCl on the device PCE were attributed to their lowered compatibility with the Pb-Sn perovskite due to their F contents, which reduced the average grain size in the surface layers of their resultant Pb-Sn perovskite films.

The mechanisms through which the addition of PH•HCl brought about the enhancements in PSC device performance were further investigated with PL spectroscopy and electrical characterizations [23, 24]. PL spectra of the Pb-Sn perovskite films (Fig. 7) reveal that the PL intensity of the PH•HCl-added perovskite film was higher than that of the pristine film, indicating that the additive effectively reduced non-radiative losses [24]. Additionally, the PL peak of the PH•HCl-added perovskite film was at slightly longer wavelengths than that of the pristine film, which was attributed to suppressed Sn^{2+} oxidation in the PH•HCl-added perovskite film. Sn^{2+} oxidation in Pb-Sn perovskite films can cause blue-shifts on PL due to its induced formation of Pb-only phases [25], and its suppression has been shown to prevent such blue-shifts, resulting in PL at longer wavelengths [26]. TRPL results shown in Fig. 7(b) and Table S1. revealed similar findings, where the PL of the PH•HCl-added perovskite film decayed distinctly more slowly, with the fitted PL lifetimes significantly longer, than did that of the pristine film. The longer PL lifetimes of the PH•HCl-added perovskite film provided further evidence to the film's reduced nonradiative recombination [24]. Conversely, PL and TRPL results on the FPH•HCl-added perovskite film (Figure S7) showed an opposite trend to that of the PH•HCl-added perovskite film; i.e. the PL intensity and lifetime were reduced upon the addition of FPH•HCl, which was attributed to the reduced grain size in the FPH•HCl-added perovskite film as discussed above.

Electrical characterizations, including EIS and SCLC measurements, of Pb-Sn PSC devices fabricated with or without the addition of PH•HCl yielded consistent observations with those from the PL results. Fig. 8(a) presents Nyquist plots obtained with EIS measurements for the with- and without-PH•HCl Pb-Sn PSC devices, with the recombination resistance

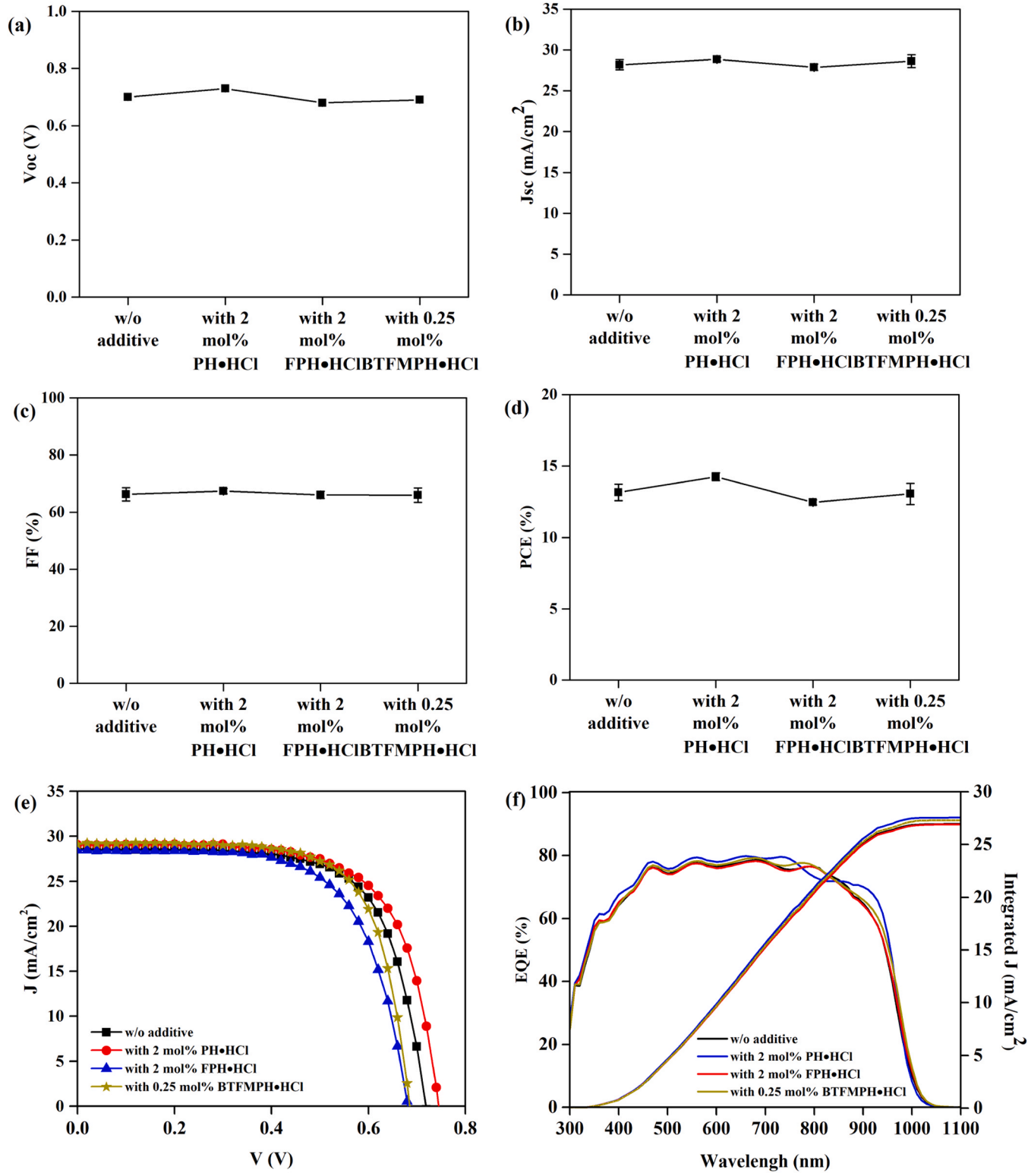

Fig. 4. Pb-Sn PSC device characteristics with or without the addition of PH•HCl, FPH•HCl, or BTFMPH•HCl at their respective optimal concentration: (a) Voc, (b) Jsc, (c) FF, (d) PCE, (e) J-V curves, and (f) external quantum efficiency (EQE) spectra.

(R_{rec}) values extracted from the Nyquist plots presented in Table S2. The EIS results revealed that the PH•HCl-added devices had a significantly higher R_{rec} than did the control (without-PH•HCl) device, again pointing to reduced recombination defects in the PH•HCl-added devices [27]. Fig. 8(b) and Fig. 8(c) present J-V curves of hole- and electron-only Pb-Sn PSC devices with- or without the addition of PH•HCl, respectively, obtained from SCLC measurements. The trap-filled limit voltages ($V_{E,\ TFL}$ and $V_{H,\ TFL}$ for electrons and holes, respectively), trap densities ($N_{t,\ Hole}$ and $N_{t,\ Electron}$ for electrons and holes, respectively), and carrier mobility (μ_h and μ_e for electrons and holes, respectively) extracted from the SCLC measurement results are summarized in Table S3. The PH•HCl-added devices showed smaller $V_{E,\ TFL}$ and $V_{H,\ TFL}$

Table 1
Pb-Sn PSC device characteristics with or without the addition of PH•HCl, FPH•HCl, or BTFMPH•HCl at their respective optimal concentration.

Pb-Sn PSCs	*Voc* (V)	*Jsc* (mA/cm^2)	FF (%)	PCE (%)	Hysteresis Ratio (%)	Champion PCE (%)
Without additive	0.70 ± 0.01	28.19 ± 0.62	66.26 ± 2.33	13.16 ± 0.58	4.68 ± 2.97	14.17
With 2 mol% PH•HCl	0.73 ± 0.01	28.86 ± 0.25	67.37 ± 0.94	14.26 ± 0.27	1.63 ± 1.28	14.74
With 2 mol% FPH•HCl	0.68 ± 0.01	27.89 ± 0.39	66.09 ± 1.24	12.45 ± 0.18	1.49 ± 1.79	12.79
With 0.25 mol% BTFMPH•HCl	0.69 ± 0.01	28.63 ± 0.79	65.95 ± 2.50	13.05 ± 0.74	9.00 ± 3.18	14.11

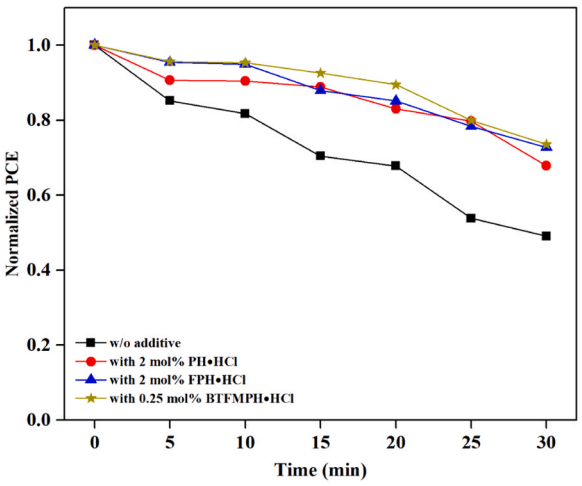

Fig. 5. PCE as a function of storage time in ambient air (~25 °C and ~70 % RH) for Pb-Sn PSC devices with or without the addition of PH•HCl, FPH•HCl, or BTFMPH•HCl at their respective optimal concentration.

than that of the control devices, with lower $N_{t,\ Hole}$ and $N_{t,\ Electron}$ but higher μ_h and μ_e, all indications of decreased defect concentration in the PH•HCl-added devices.

4. Conclusions

Three phenyl-substituted hydrazine compounds with different numbers of fluorine substituents—i.e. PH•HCl (no F substituent), FPH•HCl (1 F substituent), and BTFMPH•HCl (6 F substituents)—were tested as additives to Pb-Sn perovskite precursor solutions to examine their effects on the resultant Pb-Sn PSC devices' characteristics and stability. All of the three additives significantly improved the stability of Pb-Sn PSC devices, with the additives containing more F contents showing slightly greater improvements. The PH•HCl additive resulted in enhanced device power conversion efficiency (PCE) and reduced hysteresis ratio thanks to its multifaceted effects including improving morphology, reducing non-radiative losses, alleviating recombination defects, and enhancing charge-carrier mobility of the Pb-Sn perovskite layer, as elucidated by a series of photo-luminescence and electrical characterizations. Both the BTFMPH•HCl and FPH•HCl additives slightly degraded the device PCE due to their poorer resultant perovskite morphology, which was attributed to their lower affinity with the perovskite as a result of their F contents. Our results provide useful insights in selecting and designing hydrazine-based additives for PSC.

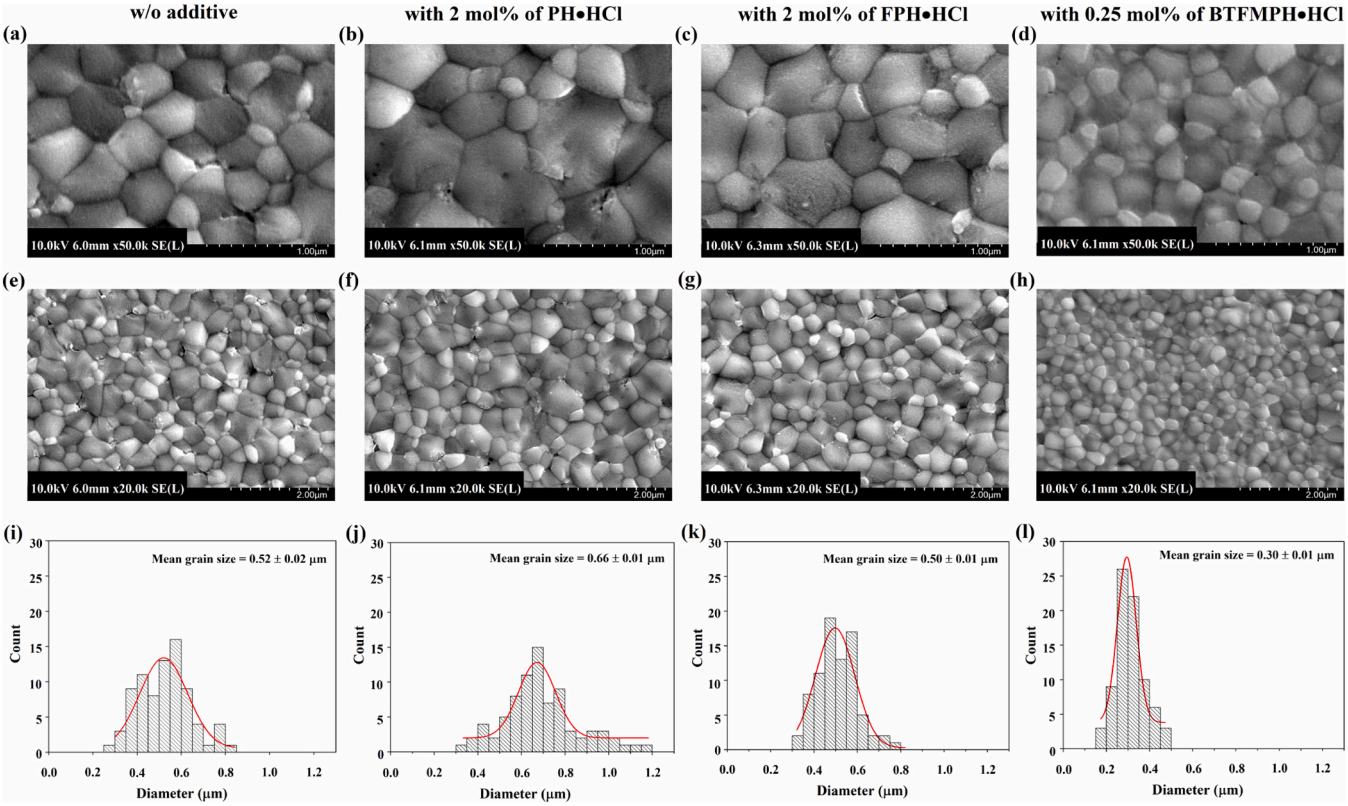

Fig. 6. (a) - (h) SEM images, and (i) - (l) grain size distribution and average grain size determined from (a) - (h), of Pb-Sn perovskite films with or without the addition of the three hydrazine compounds at their respective optimal concentrations.

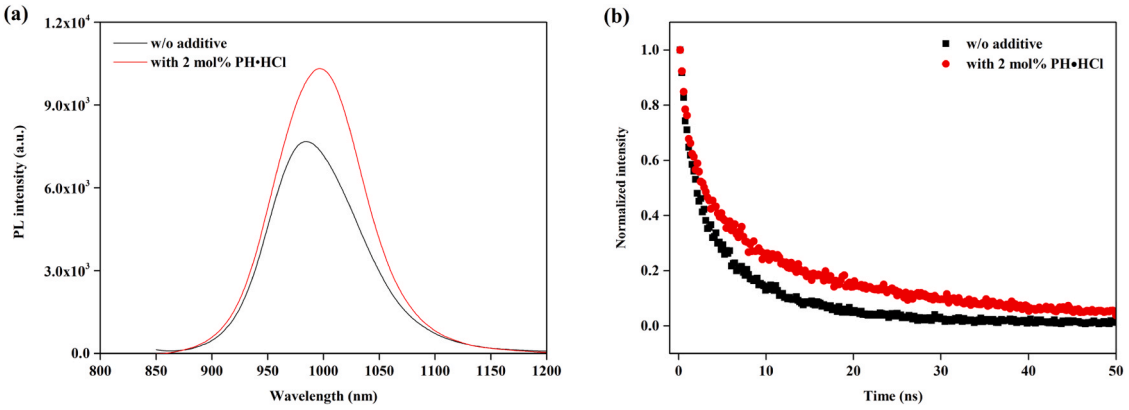

Fig. 7. (a) Photoluminescence (PL) spectra; (b) time-resolved PL (TRPL) spectra of Pb-Sn perovskite films with or without the addition of 2 mol% of PH•HCl.

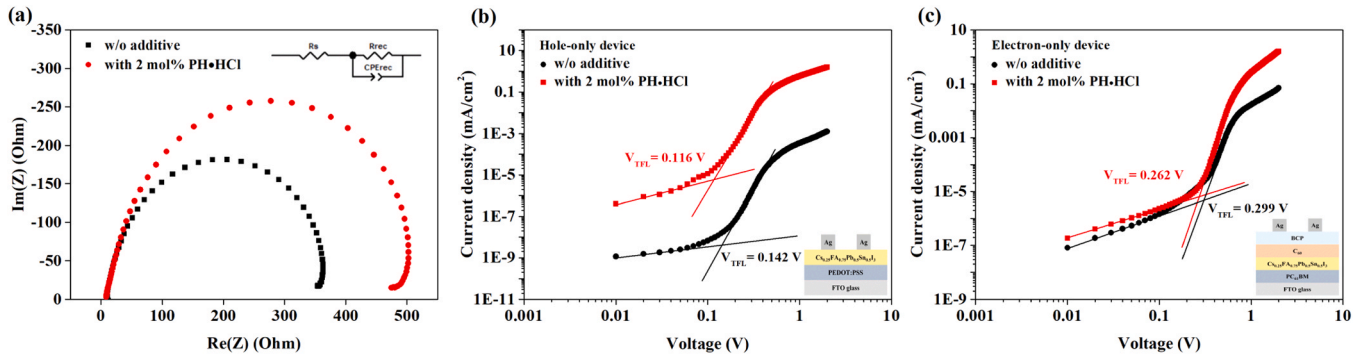

Fig. 8. (a) Nyquist plots obtained with electrochemical impedance spectroscopy (EIS) of Pb-Sn PSC devices with or without the addition of 2 mol% of PH•HCl; the inset depicts an equivalent circuit; (b) space-charge-limited current (SCLC) measurement results of hole-only devices (FTO/PEDOT:PSS/$Cs_{0.25}FA_{0.75}Pb_{0.5}Sn_{0.5}I_3$/Ag) with or without the addition of 2 mol% of PH•HCl; (c) SCLC results of electron-only devices (FTO/$PC_{61}BM$/$Cs_{0.25}FA_{0.75}Pb_{0.5}Sn_{0.5}I_3$/$C_{60}$/BCP/Ag) with or without the addition of 2 mol% of PH•HCl.

CRediT authorship contribution statement

Sheng-Wen Huang: Resources, Data curation. **Yu-Chi Chen:** Methodology, Investigation, Formal analysis, Data curation. **Chia-Feng Li:** Resources, Data curation. **Kai-Leng Huang:** Writing – original draft, Methodology, Investigation, Formal analysis, Data curation, Conceptualization. **Feng-Yu Tsai:** Writing – review & editing, Validation, Supervision, Resources, Project administration, Methodology, Investigation, Funding acquisition, Formal analysis, Data curation, Conceptualization. **Wei-Fang Su:** Resources. **Yu-Ching Huang:** Resources.

Declaration of Competing Interest

The authors declare the following financial interests/personal relationships which may be considered as potential competing interests: Feng-Yu Tsai reports financial support was provided by National Science and Technology Council of Taiwan. Feng-Yu Tsai reports financial support was provided by National Taiwan University Advanced Research Center for Green Materials Science and Technology. If there are other authors, they declare that they have no known competing financial interests or personal relationships that could have appeared to influence the work reported in this paper

Data Availability

Data will be made available on request.

Acknowledgment

This work was supported by funding provided to Feng-Yu Tsai by National Science and Technology Council of Taiwan (Grant Nos. 111-2221-E-002-026 -MY3, 111-2923-E-002-007 -MY3, 111-2923-E-002-012 -MY3, 112-2218-E-002-050 -) and by "National Taiwan University Advanced Research Center For Green Materials Science and Technology" from The Featured Area Research Center Program within the framework of the Higher Education Sprout Project by the Ministry of Education (Grant No. 112L9006).

Appendix A. Supporting information

Supplementary data associated with this article can be found in the online version at doi:10.1016/j.jallcom.2024.175832.

References

[1] P. Roy, N. Kumar Sinha, S. Tiwari, A. Khare, A review on perovskite solar cells: evolution of architecture, fabrication techniques, commercialization issues and status, Sol. Energy 198 (2020) 665–688, https://doi.org/10.1016/J.SOLENER.2020.01.080.

[2] I. Mathews, S. Sofia, E. Ma, J. Jean, H.S. Laine, S.C. Siah, T. Buonassisi, I.M. Peters, Economically sustainable growth of perovskite photovoltaics manufacturing, Joule 4 (2020) 822–839, https://doi.org/10.1016/J.JOULE.2020.01.006.

[3] S. Gu, R. Lin, Q. Han, Y. Gao, H. Tan, J. Zhu, Tin and mixed lead–tin halide perovskite solar cells: progress and their application in tandem solar cells, Adv. Mater. 32 (2020) 1907392, https://doi.org/10.1002/ADMA.201907392.

[4] G. Kapil, T. Bessho, Y. Sanehira, S.R. Sahamir, M. Chen, A.K. Baranwal, D. Liu, Y. Sono, D. Hirotani, D. Nomura, K. Nishimura, M.A. Kamarudin, Q. Shen, H. Segawa, S. Hayase, Tin-Lead perovskite solar cells fabricated on hole selective monolayers, ACS Energy Lett. 7 (2022) 966–974, https://doi.org/10.1021/ACSENERGYLETT.1C02718.

[5] Best Research-Cell Efficiency Chart | Photovoltaic Research | NREL, (n.d.). https://www.nrel.gov/pv/cell-efficiency.html (Accessed April 3, 2023).
[6] R. Lin, K. Xiao, Z. Qin, Q. Han, C. Zhang, M. Wei, M.I. Saidaminov, Y. Gao, J. Xu, M. Xiao, A. Li, J. Zhu, E.H. Sargent, H. Tan, Monolithic all-perovskite tandem solar cells with 24.8% efficiency exploiting comproportionation to suppress Sn(ii) oxidation in precursor ink, 4:10 4, Nat. Energy 2019 (2019) 864–873, https://doi.org/10.1038/s41560-019-0466-3.
[7] M.E. Kayesh, T.H. Chowdhury, K. Matsuishi, R. Kaneko, S. Kazaoui, J.J. Lee, T. Noda, A. Islam, Enhanced photovoltaic performance of FASnI3-based perovskite solar cells with hydrazinium chloride coadditive, ACS Energy Lett. 3 (2018) 1584–1589, https://doi.org/10.1021/ACSENERGYLETT.8B00645.
[8] D. Wu, P. Jia, W. Bi, Y. Tang, J. Zhang, B. Song, L. Qin, Z. Lou, Y. Hu, F. Teng, Y. Hou, Enhanced performance of tin halide perovskite solar cells by addition of hydrazine monohydrobromide, Org. Electron 82 (2020) 105728, https://doi.org/10.1016/J.ORGEL.2020.105728.
[9] T.M. Koh, T. Krishnamoorthy, N. Yantara, C. Shi, W.L. Leong, P.P. Boix, A. C. Grimsdale, S.G. Mhaisalkar, N. Mathews, Formamidinium tin-based perovskite with low Eg for photovoltaic applications, J. Mater. Chem. A Mater. 3 (2015) 14996–15000, https://doi.org/10.1039/C5TA00190K.
[10] S.J. Lee, S.S. Shin, Y.C. Kim, D. Kim, T.K. Ahn, J.H. Noh, J. Seo, S. Il Seok, Fabrication of Efficient Formamidinium Tin Iodide Perovskite Solar Cells through SnF2-Pyrazine Complex, J. Am. Chem. Soc. 138 (2016) 3974–3977, https://doi.org/10.1021/JACS.6B00142.
[11] W. Li, J. Li, J. Li, J. Fan, Y. Mai, L. Wang, Addictive-assisted construction of all-inorganic CsSnIBr2 mesoscopic perovskite solar cells with superior thermal stability up to 473 K, J. Mater. Chem. A Mater. 4 (2016) 17104–17110, https://doi.org/10.1039/C6TA08332C.
[12] S. Chen, X. Xiao, H. Gu, J. Huang, Iodine reduction for reproducible and high-performance perovskite solar cells and modules, Sci. Adv. 7 (2021), https://doi.org/10.1126/SCIADV.ABE8130.
[13] C. Wang, F. Gu, Z. Zhao, H. Rao, Y. Qiu, Z. Cai, G. Zhan, X. Li, B. Sun, X. Yu, B. Zhao, Z. Liu, Z. Bian, C.C. Huang Wang, F. Gu, Z. Zhao, H. Rao, Y. Qiu, Z. Cai, G. Zhan, X. Li, B. Sun, X. Yu, B. Zhao, Z. Liu, Z. Bian, C. Huang, Self-Repairing Tin-Based Perovskite Solar Cells with a Breakthrough Efficiency Over 11%, Adv. Mater. 32 (2020) 1907623 https://doi.org/10.1002/ADMA.201907623.
[14] J. Cao, H.L. Loi, Y. Xu, X. Guo, N. Wang, C. ki Liu, T. Wang, H. Cheng, Y. Zhu, M. G. Li, W.Y. Wong, F. Yan, High-Performance Tin–Lead Mixed-Perovskite Solar Cells with Vertical Compositional Gradient, Adv. Mater. 34 (2022) 2107729, https://doi.org/10.1002/ADMA.202107729.
[15] K. Zhang, A. Späth, O. Almora, V.M. Le Corre, J. Wortmann, J. Zhang, Z. Xie, A. Barabash, M.S. Hammer, T. Heumüller, J. Min, R. Fink, L. Lüer, N. Li, C. J. Brabec, Suppressing Nonradiative Recombination in Lead-Tin Perovskite Solar Cells through Bulk and Surface Passivation to Reduce Open Circuit Voltage Losses, ACS Energy Lett. 7 (2022) 3235–3243, https://doi.org/10.1021/ACSENERGYLETT.2C01605.
[16] T.Bin Song, T. Yokoyama, C.C. Stoumpos, J. Logsdon, D.H. Cao, M.R. Wasielewski, S. Aramaki, M.G. Kanatzidis, Importance of reducing vapor atmosphere in the fabrication of Tin-based perovskite solar cells, J. Am. Chem. Soc. 139 (2017) 836–842, https://doi.org/10.1021/JACS.6B10734.
[17] X. He, T. Wu, X. Liu, Y. Wang, X. Meng, J. Wu, T. Noda, X. Yang, Y. Moritomo, H. Segawa, L. Han, Highly efficient tin perovskite solar cells achieved in a wide oxygen concentration range, J. Mater. Chem. A Mater. 8 (2020) 2760–2768, https://doi.org/10.1039/C9TA13159K.
[18] Z. Zhang, J. Liang, J. Wang, Y. Zheng, X. Wu, C. Tian, A. Sun, Z. Chen, C.-C. Chen, Resolving mixed intermediate phases in methylammonium-free Sn–Pb alloyed perovskites for high-performance solar cells, Nano-Micro Lett. 14 (2022) 165, https://doi.org/10.1007/s40820-022-00918-1.
[19] Y.F. Chen, Z.M. Luo, C.H. Chiang, C.G. Wu, Multifunctional Ionic Fullerene Additive for Synergistic Boundary and Defect Healing of Tin Perovskite to Achieve High-Efficiency Solar Cells, ACS Appl. Mater. Interfaces 14 (2022) 46603–46614, https://doi.org/10.1021/ACSAMI.2C12785.
[20] T. Singh, T. Miyasaka, T. Singh, T. Miyasaka, Stabilizing the Efficiency Beyond 20% with a Mixed Cation Perovskite Solar Cell Fabricated in Ambient Air under Controlled Humidity, Adv. Energy Mater. 8 (2018) 1700677, https://doi.org/10.1002/AENM.201700677.
[21] Z. Zhu, J.-Q. Xu, C.-C. Chueh, H. Liu, an Li, X. Li, H. Chen, A.K.-Y. Jen, Z. Zhu, J. Xu, C. Chueh, Z. Li, A.K.-Y. Jen, H. Chen, H. Liu, X. Li, A Low-Temperature, Solution-Processable Organic Electron-Transporting Layer Based on Planar Coronene for High-performance Conventional Perovskite Solar Cells, Adv. Mater. 28 (2016) 10786–10793, https://doi.org/10.1002/ADMA.201601745.
[22] J.-Y. Seo, T. Matsui, J. Luo, J.-P. Correa-Baena, F. Giordano, M. Saliba, K. Schenk, A. Ummadisingu, K. Domanski, M. Hadadian, A. Hagfeldt, S.M. Zakeeruddin, U. Steiner, M. Grätzel, A. Abate, J. Seo, J. Luo, F. Giordano, M. Saliba, A. Ummadisingu, K. Domanski, S.M. Zakeeruddin, M. Grätzel, A. Abate, T. Matsui, J. Correa-Baena, M. Hadadian, A. Hagfeldt, K. Schenk, Ionic Liquid Control Crystal Growth to Enhance Planar Perovskite Solar Cells Efficiency, Adv. Energy Mater. 6 (2016) 1600767, https://doi.org/10.1002/AENM.201600767.
[23] W.L. Leong, Z.-E. Ooi, D. Sabba, C. Yi, S.M. Zakeeruddin, M. Graetzel, J.M. Gordon, E.A. Katz, N. Mathews, W.L. Leong, Z.-E. Ooi, D. Sabba, N. Mathews, C. Yi, S. M. Zakeeruddin, M. Graetzel, M. Gordon, A. Katz, Identifying Fundamental Limitations in Halide Perovskite Solar Cells, Adv. Mater. 28 (2016) 2439–2445, https://doi.org/10.1002/ADMA.201505480.
[24] L. Zuo, H. Guo, D.W. DeQuilettes, S. Jariwala, N. De Marco, S. Dong, R. DeBlock, D. S. Ginger, B. Dunn, M. Wang, Y. Yang, Polymer-modified halide perovskite films for efficient and stable planar heterojunction solar cells, Sci. Adv. 3 (2017) 1700106, https://doi.org/10.1126/SCIADV.1700106.
[25] W. Zhang, X. Li, S. Fu, X. Zhao, X. Feng, J. Fang, Lead-lean and MA-free perovskite solar cells with an efficiency over 20%, Joule 5 (2011) 2904–2914, https://doi.org/10.1016/j.joule.2021.09.008.
[26] C. Tian, Z. Zhang, A. Sun, J. Liang, Y. Zheng, X. Wu, Y. Liu, C. Tang, C.-C. Chen, Tuning phase stability and interfacial dipole for efficient methylammonium-free Sn-Pb perovskite solar cells, Nano Energy 116 (2023) 108848, https://doi.org/10.1016/j.nanoen.2023.108848.
[27] E. Von Hauff, D. Klotz, Impedance spectroscopy for perovskite solar cells: characterisation, analysis, and diagnosis, J. Mater. Chem. C. Mater. 10 (2022) 742–761, https://doi.org/10.1039/D1TC04727B.